IEEE Access
Multidisciplinary ⋮ Rapid Review ⋮ Open Access Journal

Received October 7, 2020, accepted October 19, 2020, date of publication October 26, 2020, date of current version November 5, 2020.

Digital Object Identifier 10.1109/ACCESS.2020.3033502

A Compact Grounded Asymmetric Coplanar Strip-Fed Flexible Multiband Reconfigurable Antenna for Wireless Applications

KODURI SREELAKSHMI[1,2], GOTTAPU SASIBHUSHANA RAO[1], (Senior Member, IEEE), AND M. N. V. S. S. KUMAR[3], (Member, IEEE)

[1]Department of Electronics and Communication Engineering, Andhra University College of Engineering (A), Andhra University, Vishakhapatnam 530003, India
[2]Department of Electronics and Communication Engineering, Raghu Engineering College, Vishakhapatnam 531162, India
[3]Department of Electronics and Communication Engineering, Aditya Institute of Technology and Management, Srikakulam 532201, India

Corresponding author: Koduri Sreelakshmi (lakshmisaibaba12@gmail.com)

ABSTRACT A compact grounded asymmetric coplanar strip (GACS)-fed flexible multiband frequency reconfigurable antenna with two PIN diodes is proposed. The investigated antenna is backed by a flexible polyamide substrate with compact dimensions of 24 mm × 19 mm and a thickness of 1.53 mm. The investigated antenna structure contains a monopole patch that facilitates operation for wireless LAN applications, whereas inverted L-shaped and F-shaped monopoles facilitate operation for Bluetooth and 5G NR applications. The investigated antenna operates at 2.4, 3.8, and 5.6 GHz with measured impedance bandwidths of 5.8%, 6.3%, and 6.6%, respectively, over the three frequency bands, thus facilitating coverage for Bluetooth, 5G NR, and WLAN standards. The two PIN diodes are employed to tune the investigated antenna among four modes, including a single band mode (WLAN 5.5 GHz), two dual-band modes (5G NR 3.8/5.6 GHz, and Bluetooth 2.48/5.6 GHz), and one multiband mode with Bluetooth (2.4 GHz), 5G New Radio (NR) N77 band (3.8 GHz), and WLAN (5.6 GHz) modes. The investigated antenna radiates unidirectionally with a peak gain of 3.73 dBi at 5.6 GHz. Measurements are carried out on the human body to investigate the behaviour of the wearable antenna. The simulated SAR values are in a safe limit of 1.6 W/kg for 1 g of tissue, according to the FCC. Moreover, the investigated antenna shows extremely low vulnerability to degradation in performance as a result of bending effects concerning impedance matching with acceptable acquiescence between measurements and simulations.

INDEX TERMS Flexible, GACS, reconfigurable, multiband, WLAN.

I. INTRODUCTION

Flexible antenna technology has received much attention with several progressing research efforts since these antennas can allow communications along curved surfaces not appropriate for traditional rigid antennas [1], [2]. With the consecutive progress of multifunction and multistandard wireless devices, reconfigurable flexible antennas have garnered much consideration due to their characteristics of reconfigurability and flexibility. Reconfigurable antennas [3], [4] and flexible materials are integrated to fabricate a reconfigurable flexible antenna that not only possesses the benefits of flexibility, significant space savings, a good carrier fit, a light weight, and a low cost but can be used to fulfil the role of numerous individual antennas. Consequently, studies of reconfigurable flexible antennas are important in complex circumstances. Presently, some methods for multiband antenna design include a compact triple-band antenna fed by a coplanar waveguide (CPW) [5], a monopole with two F-shaped slot radiators and a microstrip-fed antenna [6], a tri-band double-element folded dipole monopole-fed antenna [7], a monopole antenna for tri-band applications [8], and a compact triple-band double-planar inverted-F antenna [9]. However, these models are not flexible, and they transmit all resonances regardless of user needs. Alternatively, it is not possible to tune a multiband antenna at the required frequency. To address these constraints, researchers have designed a feasible solution: reconfigurable antennas. Reconfigurable antennas can

The associate editor coordinating the review of this manuscript and approving it for publication was Weiren Zhu.

exhibit reconfiguration properties within the appropriate radiation, frequency of operation, polarization, and combined factor ranges. Various reconfigurable antennas with distinct switching have been tested; they include a novel switchable multiband frequency reconfigurable microstrip square slot antenna [10], and a novel bowtie frequency reconfigurable antenna [11]. A reconfigurable multiband bowtie slot antenna employs switchable pairs of slots [12]. A simple multiband reconfigurable antenna with dual pairs of PIN diodes [13] and a compact quad-band reconfigurable monopole antenna [14] have also been proposed. However, not all reconfigurable antennas use active elements to achieve reconfigurable properties; there are some passive reconfigurable antennas that were reported in [15]–[17]. In [15], [16], reconfigurable pattern antennas that employ graded dielectric plates and metasurfaces to reconfigure beams in a particular direction were reported. The pattern reconfigurable monopole antenna with polarization-insensitive FSS for beam reconfigurability was reported in [17]. Currently, based on artificial intelligence techniques, antenna resonating frequencies and radiation patterns are being reconfigured, and particle swarm optimization was used in [18] to change the operating frequency. However, although these antennas are reconfigurable, the corresponding models are generally developed on rigid substrates.

For conformal applications, antennas based on rigid substrates are not appropriate. Currently, due to their robustness and light weight, flexible antennas have become popular. Several flexible antennas were reported in [19]–[35], including a low-cost inkjet-printed flexible multiband antenna [19], a flexible antenna modelled on aluminium-metalized polypropylene [20], two flexible and compact flower-shaped CPW-fed antennas [21], a compact, flexible antenna system designed for telemedicine applications [22], two ultraflexible/thin printed monopole antennas [23], a miniature fishtail-shaped antenna [24], a compact, low- volume flexible antenna with a novel structure model for wireless applications [25], a flexible broadband comb-shaped monopole antenna [26], a low-profile UWB flexible antenna [27], and a novel flexible and low-cost inkjet printed dual-band antenna, based on a customized analytic curve [28]. Although these antennas are flexible, they are either large or provide a limited number of resonances, and they are not reconfigurable.

Different reconfigurable stretchable substrate antennas were reported in [29]–[35], including a novel flexible, reconfigurable antenna built on the theory of folded slot antennas [29], [30]; however these antennas have large areas of 1829 mm^2 to 7387 mm^2 and are limited to dual-band antennas. A CPW-fed dual-polarised dual-band with discrete-frequency reconfigurability flexible monopole antenna was proposed in [31], but the presented antenna had a large area of 1650 mm^2 and is limited to dual-band cases. A flexible, reconfigurable antenna modelled on a denim substrate was proposed in [32], but the antenna had a large area of 1175 mm^2 and was limited to dual-band cases. A reconfigurable-frequency antenna modelled on flexible materials for wireless applications was proposed in [33], but the antenna had a large area of 1848 mm^2, many switches are used and it was limited to dual-band cases. A spiral-shaped CPW-fed flexible frequency reconfigurable antenna was proposed in [34], and an inkjet printed reconfigurable antenna on a paper substrate was demonstrated in [35]; however, flexibility tests were not carried out for these antennas.

A grounded asymmetric coplanar strip (GACS) is a modification of an ACS. On the back of the substrate, an additional ground plane is used. The bottom ground plane is spaced 1.53 mm beneath the top ground to decrease backward radiation. In this article, a compact, flexible multiband reconfigurable GACS-fed antenna that utilizes dual-PIN diodes (SMP 1320-079) to realize frequency reconfiguration functionality that covers the Bluetooth/IMT-E, 5G NR N77 band, and WLAN frequencies is presented. The main motivation for investigating this flexible, reconfigurable multiband antenna is the high demand for flexible electronics. Flexible substrate antennas (FSAs) are quickly becoming a preferred option for flexible displays, smart clothing, wearable computer systems, and applications in wireless sensing, such as health care monitoring, surveillance in civil construction, or inclusion in search and rescue satellite networks. Furthermore, the frequency reconfigurable antenna provides excellent out-of-band noise rejection which immensely reduces filtering demands of the front-end circuitry. Section II introduces the investigated design, a parametric study, and the principle of operation. The antenna radiation characteristics and performance are examined in Section III. Section IV discusses the functioning of the investigated antenna and the bending effect. Section V presents an SAR analysis. Section VI investigates antenna behaviour in close vicinity to the human body. A comparison of the investigated antenna and other existing models is reported in Table 7. Finally, conclusions are provided in Section VII.

II. ANTENNA DESIGN AND PARAMETRIC STUDY

A. STRUCTURE AND DIMENSIONS

The proposed tri-band flexible frequency reconfigurable antenna covering Bluetooth, 5G NR, and WLAN frequency bands is shown in Fig. 1. The compact dimensions of the substrate of the investigated antenna are 24 mm $\times$ 19 mm. The investigated antenna is formed on a 1.53-mm-thick flexible polyamide substrate, with $\varepsilon_r = 4.3$ and $\tan\delta = 0.004$. The investigated antenna includes a monopole patch connected to a 50 Ω GACS feedline for better impedance matching corners of the patch are truncated on the left-hand side, and U-shaped slot is cut on the patch at the right-hand side. An inverted L-shaped monopole, an F-shaped monopole connected to the monopole patch and two RF PIN diode switches are used. Multiband frequency reconfigurable performance is achieved for 5G NR and Bluetooth applications by turning ON/OFF the PIN diodes SW1 and SW2, respectively. Fig. 2 shows the evolution process of the investigated multiband frequency reconfigurable flexible antenna in three steps, which are examined during the simulation studies.

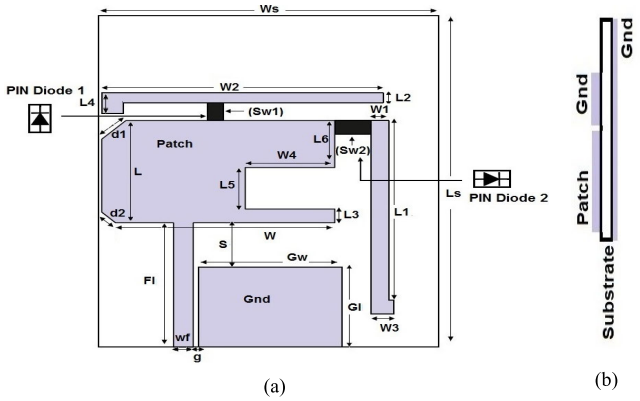

FIGURE 1. Geometrical configuration: (a) Top view and (b) Side view.

Antenna-1 is developed to function at the primary fundamental frequency of $f_{WLAN} = 5.63$ GHz. The Antenna-1 configuration includes a monopole patch joined to the 1.1-mm-wide 50 Ω GACS feedline (as illustrated in Fig. 2(a)). The optimized monopole patch length and width are estimated by (1) and (2).

$$L = \frac{c}{4f_{WLAN}\sqrt{\in_{reff}}} \tag{1}$$

$$W = \frac{c}{2f_{WLAN}\sqrt{\in_{reff}}} \tag{2}$$

$$\in_{reff} = \frac{\in_r + 1}{2}$$

where C is the speed of light, $\in_{reff}$ is the effective relative permittivity of the substrate and f_{WLAN} is the WLAN operating frequency. The monopole patch has a theoretical length value at $f_{WLAN} = 5.63$ GHz of L = 8.2 mm, and the optimized value is L = 7.4 mm. Additionally, theoretical width value is W = 16.3 mm at $f_{WLAN} = 5.63$ GHz, and the optimized value W = 13 mm.

Antenna-2 is optimized to operate at a second resonance frequency of $f_{Bluetooth} = 2.45$ GHz to provide Bluetooth frequency band services. The Antenna-2 configuration includes an inverted L-shaped monopole connected to a monopole patch (as illustrated in Fig. 2(b)). The inverted L-shaped monopole length is estimated by (3):

$$L1 = \frac{c}{4f_{Bluetooth}\sqrt{\in_{reff}}} \tag{3}$$

where C is the speed of light, $\in_{reff}$ is the effective relative permittivity of the substrate, and $f_{\text{Bluetooth}}$ is the Bluetooth operating frequency. The monopole has a theoretical length of L1 = 18.8 mm, and the optimized value is L1 = 14 mm.

Moreover, a PIN diode (SW2) is embedded between the monopole patch and inverted L-shaped radiating monopole to provide flexible frequency reconfigurable performance at 2.45 GHz. In the forward bias condition (ON state), the RF PIN diode is represented as a series of resistance ($R_S = 1\Omega$) and inductance (L = 0.6 nH) components, and in the reverse bias condition (OFF state), it is represented as a parallel blend of a resistor (Rs = 0.1 kΩ) and capacitor ($C_R = 0.1$ pF)

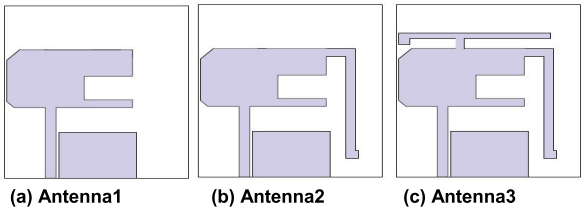

FIGURE 2. Evolution of the investigated antenna.

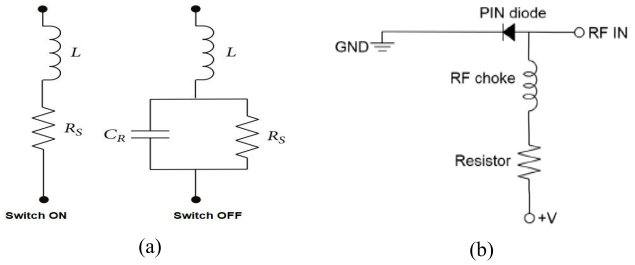

FIGURE 3. RF PIN diode: (a) Electrical model and (b) Biasing circuit.

with an inductor (L = 0.6 nH) in series. In the OFF state, PIN diode SW2 facilitates functioning at the WLAN frequency, and it facilitates functioning at both the WLAN and Bluetooth frequency bands for the ON condition. Furthermore, an RF PIN diode (SW1) and F-shaped radiating monopole are used to achieve second frequency reconfigurable operation at $f_{5G} = 3.65$ GHz and contribute services within the 5G NR N77 frequency band, as illustrated in Fig. 2(c) (Antenna-3). The radiating F-shaped monopole length is calculated using (4):

$$W2 = \frac{c}{4f_{5G}\sqrt{\in_{reff}}} \tag{4}$$

where C is the speed of light, $\in_{reff}$ is the effective relative permittivity of the substrate and f_{5G} is the 5G NR operating frequency. The monopole has a theoretical length value of W2 = 12.6 mm, and the optimized value is W2 = 15.7 mm.

Figure 3(a) illustrates a PIN diode and the corresponding circuitry. The biasing circuit consists of a 10-μH inductor (from Murata Technology) used as a radio-frequency choke to keep the radio-frequency signal from influencing the DC bias lines, and a resistor of 1 Ω is mounted on the fabricated antenna to regulate the DC biasing current through the PIN diode, as illustrated in Fig. 3(b). Table 1 provides optimized dimensions for the investigated antenna. The simulated S_{11} characteristics of the presented antenna at different steps in the development process are illustrated in Fig. 4. Table 2 provides simulation results for the investigated flexible tri-band antenna at different steps in the development process.

B. PARAMETRIC STUDY

The inverted L-shaped monopole length (L1) has an important effect on the operating frequency. The optimum inverted L-shaped monopole length is determined by performing a parametric study. The results are illustrated in Fig. 5. Furthermore, as the inverted L-shaped stub length L1 increases,

TABLE 1. Investigated antenna dimensions in millimeters.

Ls	24	L	7.4
Ws	19	W	13
Gw	8	L5	3
Gl	5.8	W4	5
wf	1.1	L3	1
Fl	9	d1	1,9
g	0.3	d2	1
L1	14	L6	3.4
W1	1	W2	15.7
W3	1.3	L2	0.7
L4	1.5	S	3.2

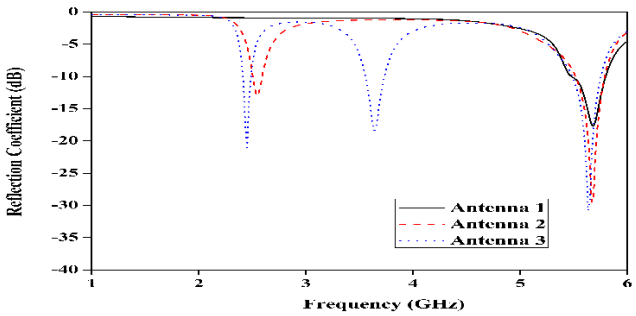

FIGURE 4. Simulated S_{11} characteristics at different steps in antenna evolution.

TABLE 2. Simulated performance studies for the investigated antenna.

Configuration	Operating frequency (GHz)	Reflection coefficient (dB)	Bandwidth (MHz)	Gain (dBi)
Antenna-1	5.68	-17.75	330	3.92
Antenna-2	2.54	-13	90	1.96
	5.67	-30.7	280	3.96
Antenna-3	2.45	-21.4	100	2.3
	3.65	-18.2	180	3.33
	5.63	-30.8	280	3.96

there is an enhancement in S_{11} for the investigated antenna. Additionally, the operating frequency decreases as the dimension of L1 is increased from 13 mm to 15 mm because the length L1 is inversely related to the centre frequency of the frequency band. The variation in the L1 does not change bandwidth. Furthermore, the length L1 has an eminent effect on the operating frequency; changing the length from 13 to 15 mm moves the resonant frequency approximately from 2.55 to 2.35 GHz. Furthermore, to achieve an operating frequency centred at 2.45 GHz (devoted to the Bluetooth operations), the length L1 should be optimized (L1 = 14 mm).

III. RESULTS AND ANALYSIS

Flexible and reconfigurable antenna simulations were performed with Ansys HFSS software. Furthermore, the simulated and measured S_{11} values were obtained for various switch conditions (SW1 and SW2), and the surface current distribution was studied at the three operating frequencies to obtain a good understanding of tri-band operation for the presented antenna, as illustrated in Fig. 6. After optimizing

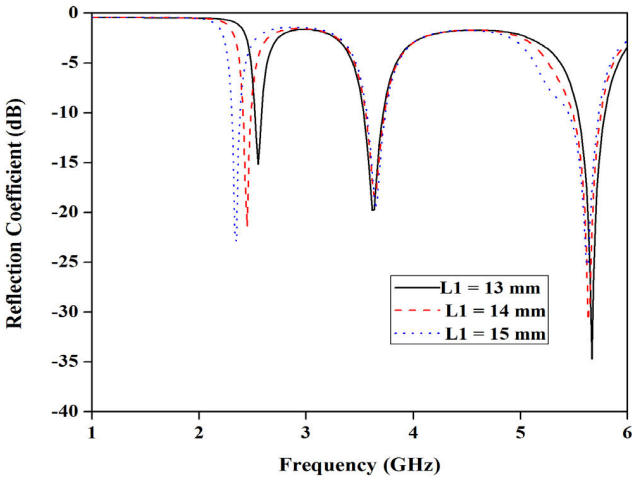

FIGURE 5. Variation in S_{11} with changes to L1.

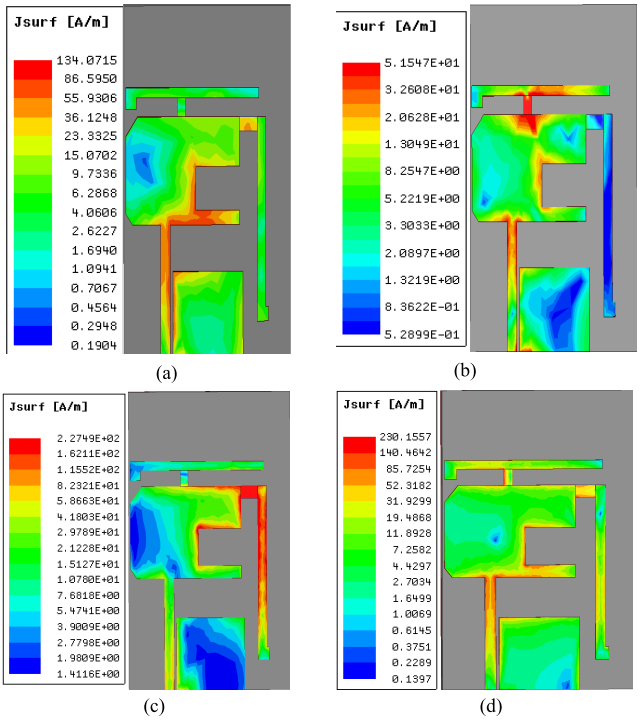

FIGURE 6. The normalized magnitude current distribution of the investigated antenna at resonant frequencies: a) 5.5GHz (Mode 1), b) 3.8 GHz (Mode 2), c) 2.4 GHz (Mode 3), and d) Mode 4.

the antenna parameters, an experimental model of the investigated antenna was developed to justify the simulated results. A photograph of the manufactured antenna integrated with the biasing circuit and the experimental setup is illustrated in Fig. 7.

A. SW1 AND SW2 OFF (MODE 1)

Fig. 6(a) demonstrates the current distribution of the flexible, reconfigurable antenna in this mode. As observed in Fig. 6(a), the maximum current is extremely concentrated throughout the monopole patch, ground and feedline. Fig. 8 demonstrates

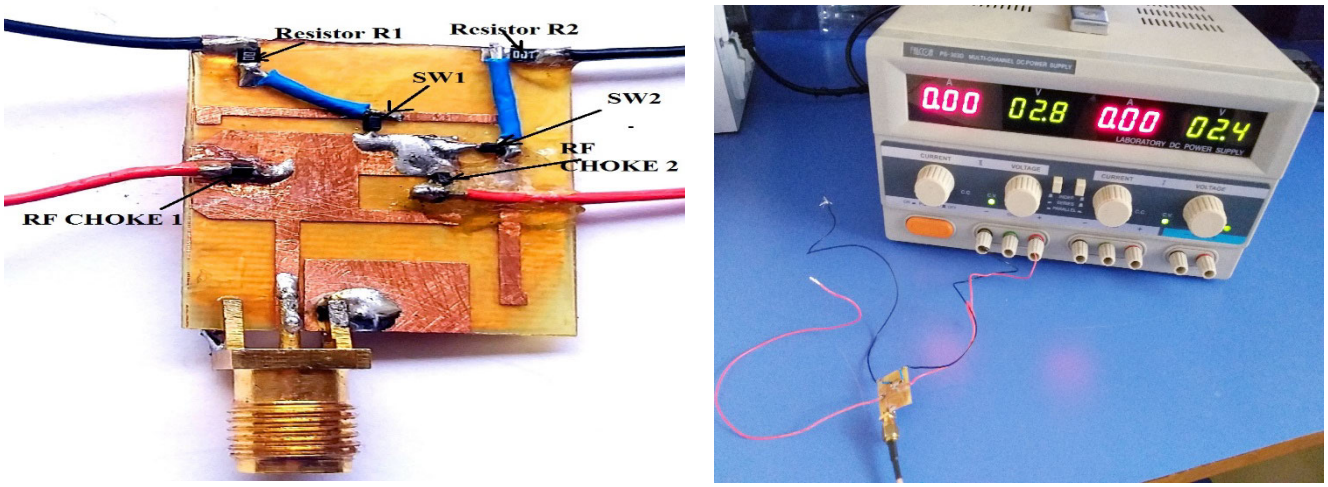

FIGURE 7. Fabricated model of the investigated antenna with a biasing circuit and the experimental setup.

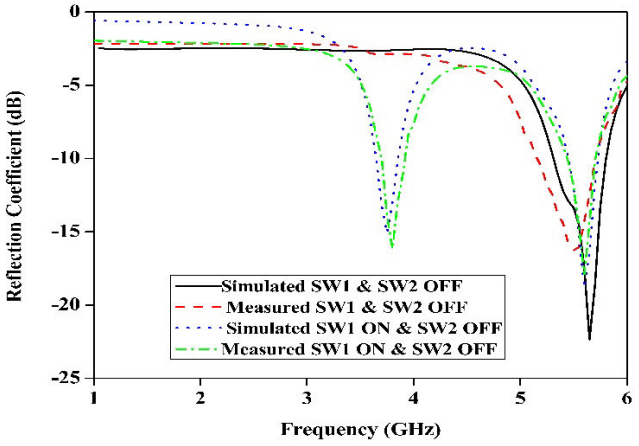

FIGURE 8. Simulated and measured S_{11} values for the different modes of operation for PIN diodes in Mode 1 and Mode 2.

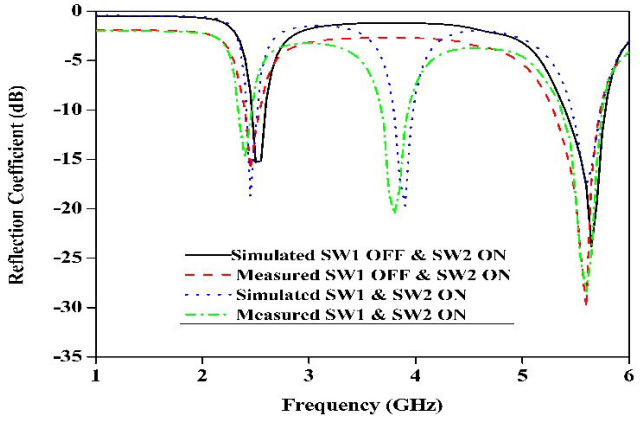

FIGURE 9. Simulated and measured S_{11} values for the different modes of operation for PIN diodes in Mode 3 and Mode 4.

the measured and simulated S_{11} characteristics of the investigated antenna with PIN diodes SW1 and SW2 in the OFF state. A single frequency band is observed at 5.5 GHz with a maximum S_{11} of −16.25 dB. The bandwidth of the first band is 10.1%, which is used for WLAN tasks.

B. SW1 ON AND SW2 OFF (MODE 2)

Fig. 6(b) demonstrates the current distribution for the flexible, reconfigurable antenna in this mode. As shown in Fig. 6(b), the maximum current is extremely concentrated throughout the monopole patch, and an F-shaped monopole is observed. Fig. 8 demonstrates the measured and simulated S_{11} characteristics of the investigated antenna for the ON state of PIN diode SW1 and the OFF state of SW2. Dual-frequency bands are noted at 3.8 GHz and 5.6 GHz, with maximum S_{11} values of −16.14 dB and −17.9 dB, respectively. The bandwidth of the first band is 6%, and this band is used for 5G NR; the bandwidth of the second band is 5.4%, and this band is used for WLAN tasks.

C. SW1 OFF AND SW2 ON (MODE 3)

Fig. 6(c) demonstrates the current distribution for the flexible, reconfigurable antenna in this mode. As shown in Fig. 6(c), the maximum current is extremely concentrated throughout the monopole patch, and an inverted L-shaped monopole can be observed. Fig. 9 illustrates the measured and simulated S_{11} characteristics of the investigated antenna with SW1 OFF and SW2 ON. Dual-frequency bands are noted at 2.48 GHz and 5.6 GHz, with maximum S_{11} values of −16.09 dB and −29.99 dB, respectively. The bandwidth of the first band is 6.1%, and this band is used for Bluetooth; the bandwidth of the second band is 8.2%, and this band is used for WLAN tasks.

D. SW1 ON AND SW2 ON (MODE 4)

Fig. 6(d) demonstrates the current distribution for the flexible, reconfigurable antenna in this mode. Fig. 9 demonstrates the measured and simulated S_{11} characteristics for the investigated flexible, reconfigurable antenna with diodes SW1 and SW2 ON. Three frequency bands are noted at

TABLE 3. Impedance bandwidths and gains of the presented antenna during different operational modes for pin diodes SW1 and SW2.

Model	Mode	Operational frequency band (GHz)	Reflection coefficient (dB)	Bandwidth (GHz)	Bandwidth (%)	Gain (dBi)
Simulated	1	5.6	-22.34	5.26-5.76	9.1	3.92
	2	3.75	-15.07	3.65-3.86	5.6	3.33
		5.6	-18.79	5.45-5.73	5	3.92
	3	2.5	-15.27	2.46-2.59	5.1	1.96
		5.65	-23.79	5.4-5.78	6.8	3.92
	4	2.45	-18.7	2.41-2.52	4.5	2.3
		3.87	-19.7	3.79-3.98	5	3.32
		5.6	-17.5	5.46-5.74	5	3.92
Measured	1	5.5	-16.25	5.15-5.7	10.1	3.82
	2	3.8	-16.14	3.7-3.93	6	3.15
		5.6	-17.9	5.42-5.72	5.4	3.71
	3	2.48	-16.09	2.38-2.53	6.1	1.83
		5.6	-29.99	5.28-5.73	8.2	3.70
	4	2.4	-14.8	2.33-2.47	5.8	2.26
		3.8	-20.5	3.68-3.92	6.3	3.14
		5.6	-28.4	5.38-5.75	6.6	3.73

TABLE 4. Investigated antenna reflection coefficient and impedance bandwidth comparison in different bent configurations for modes 1 and 4 with pin diodes.

Convex configuration with different radii		Mode	Operating frequency (GHz)	Reflection coefficient (dB)	Bandwidth	Frequency (MHz) shift towards
Bent by 15 mm	Simulated	1	5.5	-35.47	5.37-5.72	100 (lower end)
		4	2.55	-17.37	2.51-2.59	100 (higher end)
			4.0	-21.22	3.91-4.11	130 (higher end)
			5.55	-25.7	5.43-5.68	50 (lower end)
	Measured	1	5.45	-18.35	5.07-5.65	50 (lower end)
		4	2.45	-16.08	2.38-2.53	50 (higher end)
			3.85	-21.72	3.72-3.98	50 (higher end)
			5.55	-29.6	5.28-5.73	50 (lower end)
Bent by 30 mm	Simulated	1	5.45	-21.7	5.37-5.7	150 (lower end)
		4	2.55	-18.7	2.47-2.59	100 (higher end)
			4.05	-22.7	3.95-4.14	180 (higher end)
			5.55	-19.12	5.45-5.69	50 (lower end)
	Measured	1	5.4	-19.85	4.98-5.67	100 (lower end)
		4	2.5	-17.58	2.42-2.6	100 (higher end)
			3.9	-23.23	3.72-4.12	100 (higher end)
			5.5	-31.1	5.12-5.7	100 (lower end)

2.4 GHz, 3.8 GHz, and 5.6 GHz, with maximum S_{11} values of −14.8 dB, −20.5 dB, and −28.4 dB, respectively. The fractional bandwidth of the initial band is 5.8%, and this band is utilized for Bluetooth; second and third bands display 6.3% and 6.6% fractional bandwidths, respectively, thus supporting fixed 5G NR and WLAN applications. The measured and simulated bandwidths and gains of the investigated antenna under different conditions in the operation of dual PIN diodes are listed in Table 3.

Fig. 10(a) presents a snapshot of the Agilent VNA N9923A with the S_{11} characteristics of the investigated flexible and reconfigurable antenna measured with both diodes OFF (Mode 1), and Fig. 10(b) presents measured S_{11} characteristics with both diodes ON (Mode 4). Negligible dissimilarity is observed between measured and simulated S_{11} values that might be produced due to defects while soldering the PIN diodes and SMA connectors, during antenna fabrication or while connecting measurement devices and the antenna. The required bandwidths are achieved by all the operational frequency bands allocated to them per the regulatory bodies; thus, antennas relevant for different wireless applications are obtained. Fig. 11 illustrates the measured and simulated 2D normalized radiation characteristics of the investigated antenna. The investigated antenna has a unidirectional radiation pattern in the E- and H-planes. In Fig. 11, the H-plane radiation pattern tilts across nearly 30° in the direction normal to the patch geometry, and in the E-plane pattern, the major lobe tilts at −40°; additionally, a small minor lobe is present opposite this location at 5.6 GHz.

The investigated antenna has radiation efficiencies of 74%, 78%, and 90% at 2.45, 3.87, and 5.6 GHz, respectively. The investigated antenna has simulated gains of 2.3, 3.32, and 3.92 dBi at 2.45, 3.87, and 5.6 GHz and measured gains of 2.26, 3.14, and 3.73 dBi at 2.4, 3.8, and 5.6 GHz, respectively, as demonstrated in Fig. 12.

IV. BENDING ANALYSIS

The feasible utilization of the investigated antenna in flexible and bendable devices requires sufficient functionality for bent shapes. Therefore, the investigated antenna was curved in the convex directions for different radii of R1 = 15 mm and R2 = 30 mm, as illustrated in Fig. 13(a)-(b).

(a)

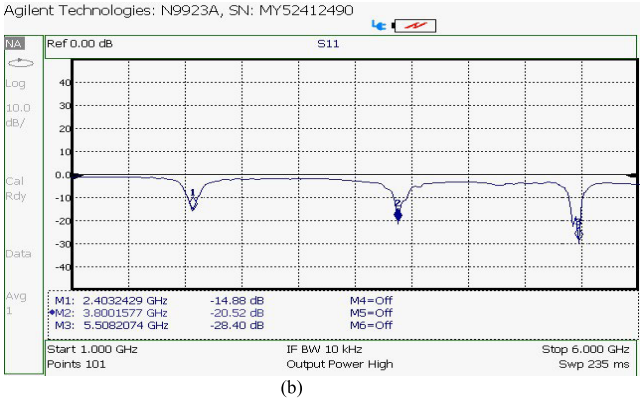

(b)

FIGURE 10. **Snapshot of the Agilent Fieldfox VNA (Model No: N9923A) with the measured S_{11} values for the investigated flexible multiband antenna: a) with both diodes SW1 and SW2 OFF and (b) with both diodes SW1 and SW2 ON.**

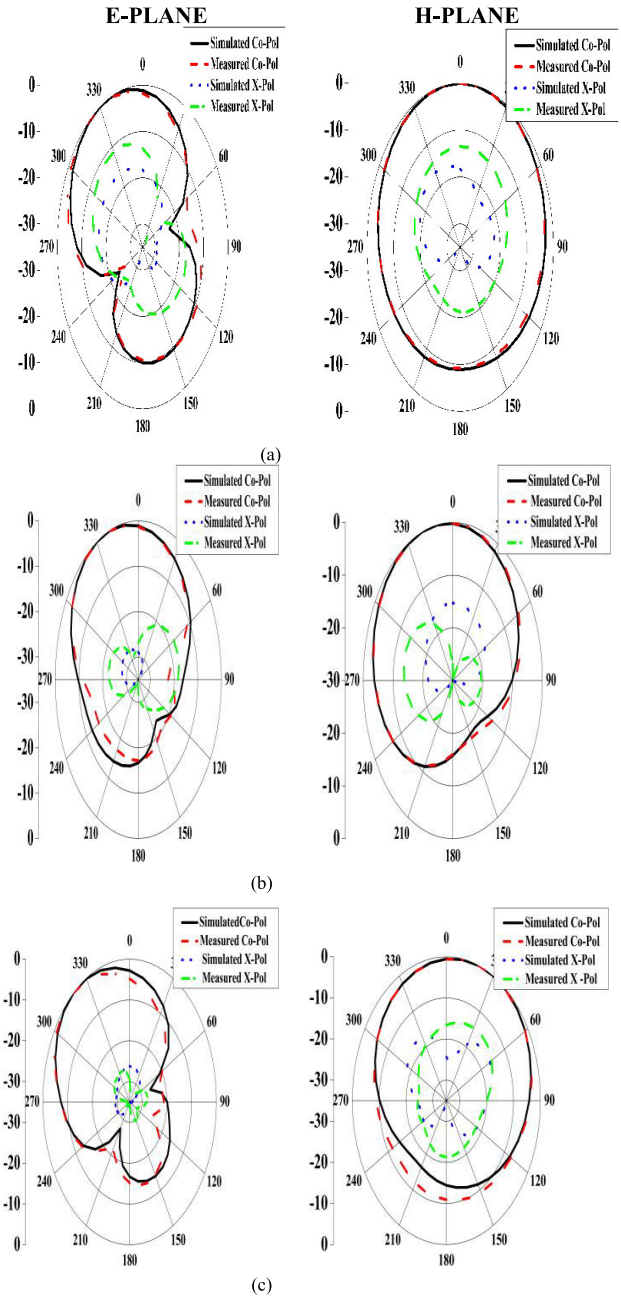

FIGURE 11. **Simulated and measured 2D radiation patterns for Mode 4 operation with PIN diodes at a) 2.4 GHz, b) 3.8 GHz, and c) 5.6 GHz.**

To justify the S_{11} and radiation patterns, a foam cylinder with radii of R1 = 15 mm and R2 = 30 mm was employed, as illustrated in Fig. 14. The foam cylinder had a negligible impact on the investigated antenna performance because the material had relative permittivity close to that of the air ($\varepsilon r = 1$).

For convex configurations with bending radii of R1 = 15 mm and R2 = 30 mm, the measured and simulated S_{11} values for the various modes of the two PIN diodes are illustrated in Fig. 15 and Fig. 16. From the bending analysis, no considerable differences among S_{11} values were found, but there was a slight drift in the operating frequencies in some cases. Table 4 lists the bending performance results for the presented flexible,reconfigurable antenna for two modes of operation with PIN diodes.

V. EVALUATION OF SAR

To study the behaviour of the investigated flexible, reconfigurable multiband antenna when placed on the human body, a specific absorption rate was numerically explored. SAR is a measure of EM wave penetration in the human body. The typical SAR level value is approximately 1.6 W/kg for 1 gram of tissue following the Federal Communication Commission (FCC) standard [36]; this value was used to calculate the SAR level in this study.

Fig. 17 illustrates a four-layered body model (100 mm x 100 mm x 40 mm) designed in HFSS, and the antenna is placed on this model with a gap of 1 mm to study the SAR level for the presented flexible antenna. The material properties of these layers are given in Table 5.

The simulated peak SAR values under different incident powers at various frequencies for mode 4 are listed in Table 6. The SAR level was increased by amplifying the incident

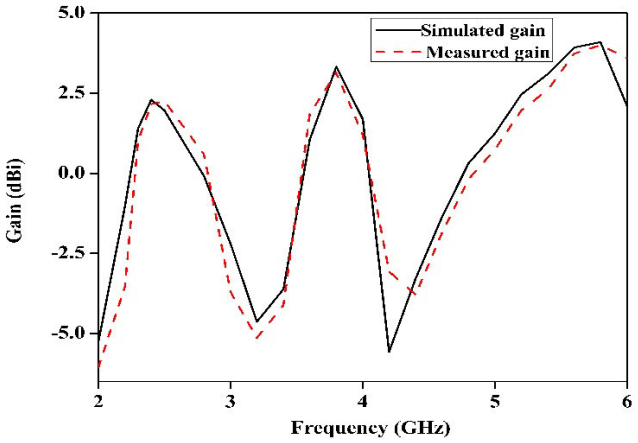

FIGURE 12. Measured and simulated gains for Mode 4 operation with PIN diodes.

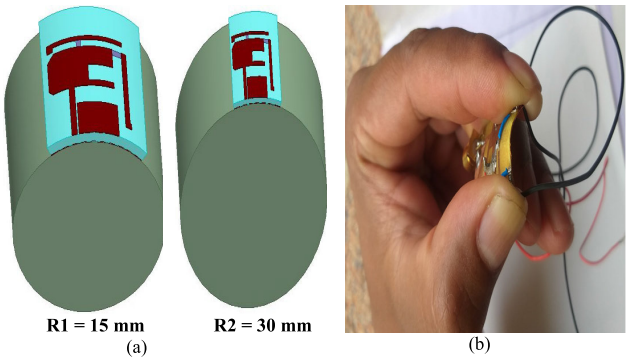

FIGURE 13. (a) The simulation design related to different bending radii. (b) Fabricated antenna with width wise bending.

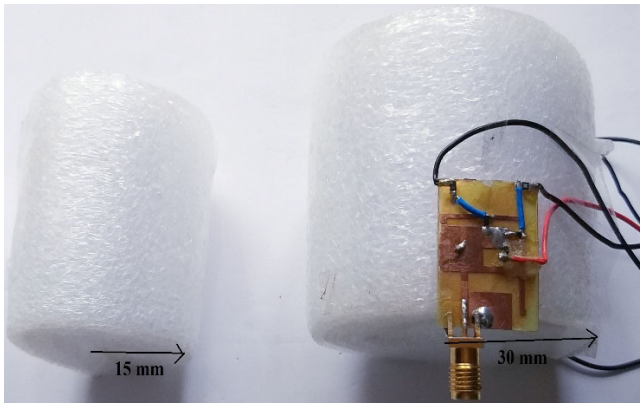

FIGURE 14. The measurement model related to different bending radii.

TABLE 5. Specifications of human body layers.

Layer	Skin	Fat	Muscle	Bone
Permittivity (ε_r)	37.95	5.27	52.67	18.49
Density (kg/m^3)	1001	900	1006	1008
Thickness (mm)	2	5	20	13
Conductivity (S/m)	1.49	0.11	1.77	0.82

power from 25 mW to 100 mW. Fig. 18 shows that at frequencies of 2.4 GHz, 3.8 GHz, and 5.6 GHz, the maximum SAR values averaged over 1 g of tissue for mode 4 are

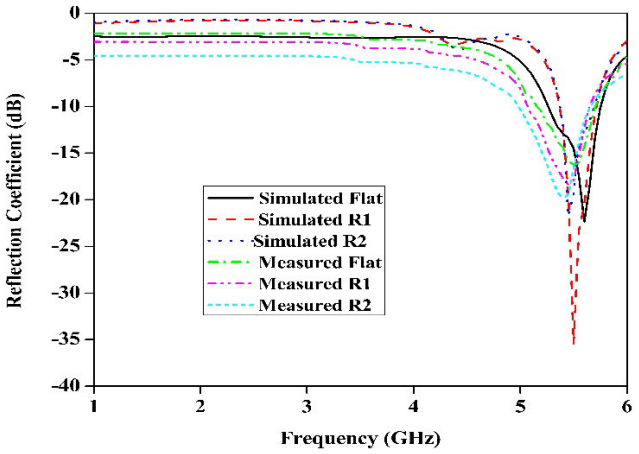

FIGURE 15. Simulated and measured S_{11} values for the presented antenna under flat and bending conditions in Mode 1.

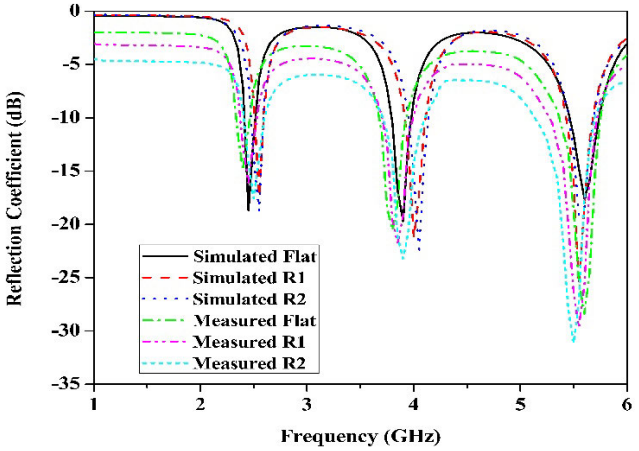

FIGURE 16. Simulated and measured S_{11} values for the presented antenna under flat and bending conditions in Mode 4.

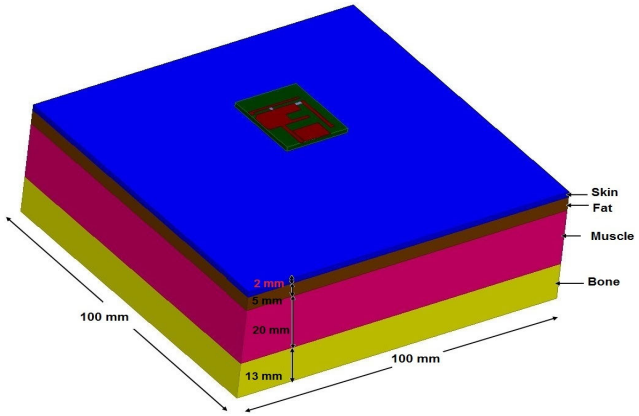

FIGURE 17. Structure of the investigated antenna placed on a four-layer human body biological model with a spacing of 1 mm.

0.25 W/kg, 0.30 W/kg, and 0.85 W/kg, respectively (at an input power of 100 mW), per the SAR IEEE C 95.1-2005 standard; the peak levels of SAR levels were still below 1.6 W/kg.

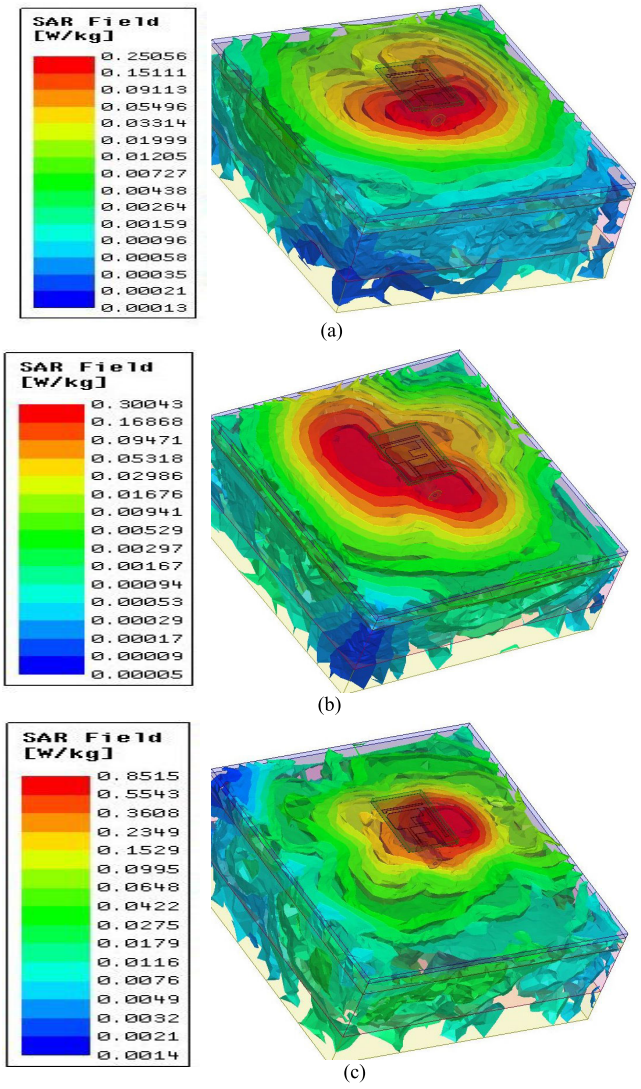

FIGURE 18. Simulated 1-gram averaged SAR patterns at a) 2.4 GHz, b) 3.8 GHz, and c) 5.6 GHz (at an input power of 100 mW) for Mode 4.

TABLE 6. Simulated peak 1-gram SAR value in w/kg.

Centre frequency (GHz)	Incident power (mW)			
	25	50	100	150
2.4	0.06	0.12	0.25	0.37
3.8	0.07	0.15	0.30	0.45
5.6	0.21	0.42	0.85	1.27

VI. ANTENNA PERFORMANCE IN THE VICINITY OF THE HUMAN BODY

The four-layered model illustrated in Fig. 17 is employed to investigate the behaviour of the presented antenna when it is placed in close vicinity to the human body. Fig. 19 illustrates the simulated S_{11} results for various gaps between the investigated antenna and four-layer body model for mode 4.

The fabricated prototype of the investigated antenna was arranged on a real human body to study the impact of the human body, as illustrated in Fig. 20. Fig. 21 illustrates the measured S_{11} values in ON and OFF body states. Due to the high relative permittivity, loss promotion, and

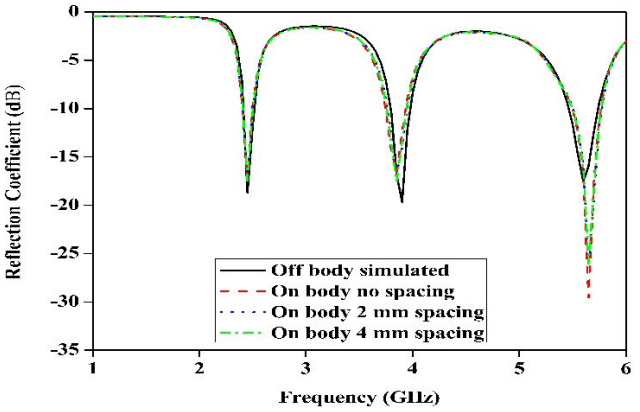

FIGURE 19. Simulated S_{11} values for various gaps between the investigated antenna and the four-layered human body model for Mode 4.

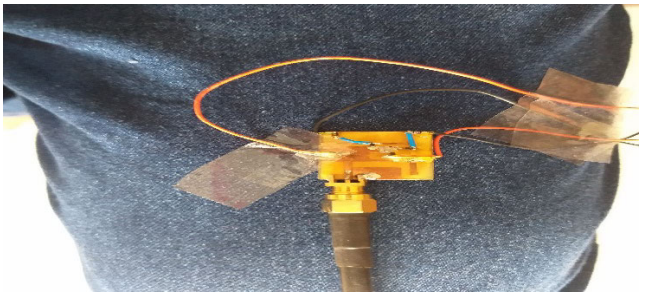

FIGURE 20. Fabricated antenna on the human body.

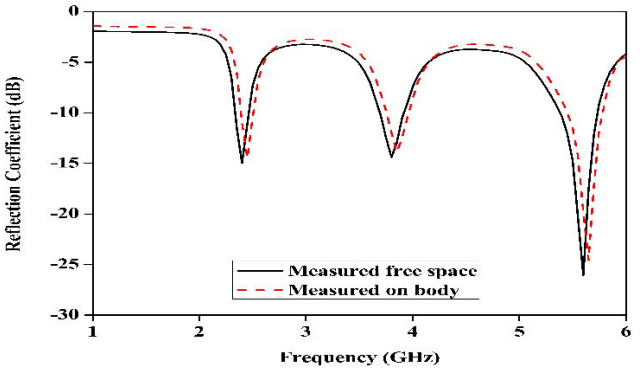

FIGURE 21. Measured S_{11} values for body V's free space for Mode 4.

frequency- dispersive nature of the human body, there is negligible dissimilarity between the S_{11} values measured under ON-body and OFF-body conditions. The investigated antenna in ON-body state has radiation efficiencies of 69%, 74%, and 83% at 2.45, 3.87, and 5.6 GHz, respectively. The investigated antenna in ON-body state has measured gains of 1.9, 2.82, and 3.52 dBi at 2.4, 3.8, and 5.6 GHz, respectively.

The proposed reconfigurable multiband antenna was compared with the previous designs to assess the novelty of the proposed device. Table 7 outlines the comparison. The presented antenna provides tri-band resonance with features of flexibility, reconfigurability, a small antenna size, and good gain.

TABLE 7. Performance evaluation of the presented work and other existing work.

Ref.	Substrate	Area(mm^2)	No. of Resonances	Operating frequencies (GHz)	Bandwidth (GHz)	Gain (dBi)	Flexibility	Reconfigurability
[7]	FR4	7480	3	1.8/2.4/3.5	1.53-1.97/2.22-2.56/ 3.31-4	4.31/3.02/5.34	No	No
[12]	FR4	2400	3	2.4/3.5/5.8	2.37-2.51/3.28-3.54/ 4.96-6.43	-	No	Yes
[19]	Polyamide	4900	4	1.2/2.0/2.6/3.4	0.18-1.5/1.93-2.2/2.31-2.96/ 3.11-3.58	-/-1.2/0.6/2.1	Yes	No
[22]	Polyamide	1350	1	2.45	-	4.8	Yes	No
[24]	PTFE	1250	2	3.5/13.8	3.4-3.6/7.4-14.4	-	Yes	No
[25]	Polyamide	990	2	2.65/3.51	2.55-2.71/3.23-4.32	2.39/1.75	Yes	No
[28]	PET film	1800	2	2.45/5.8	1.86-2.63/5.09-8.0	1.81/3.92	Yes	No
[29]	PET	1829	2	2.36/3.64	2.27-2.45/3.5-3.77	-	Yes	Yes
Proposed Work	polyamide	456	3	2.4/3.8/5.6	2.33-2.47/3.68-3.92/5.38-5.75	2.26/3.14/3.73	yes	yes

VII. CONCLUSION

A compact but flexible reconfigurable multiband antenna has been investigated in this paper. The proposed antenna is appropriate for 2.4-GHz Bluetooth, 3.8-GHz 5G NR, and 5.6-GHz WLAN applications. The antenna incorporates a monopole patch, an inverted L-shaped monopole, and an F-shaped monopole that covers the WLAN frequency band, Bluetooth frequency band, and 5G NR frequency band. Two PIN diodes are employed to reconfigure the antenna. The presented antenna shows nearly unidirectional radiation characteristics along the E-plane and the H-plane. The peak SAR levels were 0.25 W/kg, 0.30 W/kg, and 0.85 W/kg at frequencies of 2.45 GHz, 3.87 GHz, and 5.65 GHz, respectively, and these values are within safe limits according to the FCC. Furthermore, the fabricated model of the investigated antenna was investigated for the flat and convex bent shapes and on the human body, and the results verified that the functionality of the investigated antenna remains unchanged; thus, the investigated antenna is flexible, reconfigurable and relevant for wireless applications.

REFERENCES

[1] H. Khaleel, *Innovation in Wearable and Flexible Antennas*. Boston, MA, USA: WIT Publishing, 2015.
[2] B. Mohamadzade, R. M. Hashmi, R. B. V. B. Simorangkir, R. Gharaei, S. Ur Rehman, and Q. H. Abbasi, "Recent advances in fabrication methods for flexible antennas in wearable devices: State of the art," *Sensors*, vol. 19, no. 10, p. 2312, May 2019.
[3] J. Bernhard, *Reconfigurable Antennas*. San Rafael, CA, USA: Morgan & Claypool, 2007.
[4] J. Costantine, Y. Tawk, S. E. Barbin, and C. G. Christodoulou, "Reconfigurable antennas: Design and applications," *Proc. IEEE*, vol. 103, no. 3, pp. 424–437, Mar. 2015.
[5] A. W. M. Saadh and R. Poonkuzhali, "A compact CPW fed multiband antenna for WLAN/INSAT/WPAN applications," *Int. J. Electron. Commun. (AEÜ)*., vol. 109, pp. 128–135, Sep. 2019.
[6] A. K. Gautam, L. Kumar, B. K. Kanaujia, and K. Rambabu, "Design of compact F-shaped slot triple-band antenna for WLAN/WiMAX applications," *IEEE Trans. Antennas Propag.*, vol. 64, no. 3, pp. 1101–1105, Mar. 2016.
[7] J. Park, M. Jeong, N. Hussain, S. Rhee, P. Kim, and N. Kim, "Design and fabrication of triple-band folded dipole antenna for GPS/DCS/WLAN/WiMAX applications," *Microw. Opt. Technol. Lett.*, vol. 61, no. 5, pp. 1328–1332, 2019.
[8] L. Kang, X. Shi, X. H. Wang, and H. Wang, "Compact ACS-fed monopole antenna with rectangular SRRs for tri-band operation," *Electron. Lett.*, vol. 50, no. 16, pp. 1112–1114, Jul. 2014.
[9] Y. Zhang, D. Wang, L. Zhang, and M. S. Tong, "A modified planar inverted-F antenna with triple-band for Wi-Fi and LTE applications," *Prog. Electromagn. Res. M.*, vol. 73, pp. 173–181, Sep. 2018.
[10] M. Borhani, P. Rezaei, and A. Valizade, "Design of a reconfigurable miniaturized microstrip antenna for switchable multiband systems," *IEEE Antennas Wireless Propag. Lett.*, vol. 15, pp. 822–825, 2016.
[11] T. Li, H. Zhai, X. Wang, L. Li, and C. Liang, "Frequency-reconfigurable bow-tie antenna for Bluetooth, WiMAX, and WLAN applications," *IEEE Antennas Wireless Propag. Lett.*, vol. 14, pp. 171–174, 2015.
[12] A. Mansoul and M. L. Seddiki, "Multiband reconfigurable bowtie slot antenna using switchable slot extensions for WiFi, WiMAX, and WLAN applications," *Microw. Opt. Technol. Lett.*, vol. 60, no. 2, pp. 413–418, Feb. 2018.
[13] Y. I. Abdulraheem, G. A. Oguntala, A. S. Abdullah, H. J. Mohammed, R. A. Ali, R. A. Abd-Alhameed, and J. M. Noras, "Design of frequency reconfigurable multiband compact antenna using two PIN diodes for WLAN/WiMAX applications," *IET Microw., Antennas Propag.*, vol. 11, no. 8, pp. 1098–1105, Jun. 2017.
[14] K. Sreelakshmi and G. S. Rao, "Reconfigurable quad-band antenna for wireless communication," *J. Electr. Eng. Technol.*, vol. 15, no. 5, pp. 2239–2249, Sep. 2020.
[15] U. M. Afzal, A. Lalbakhsh, and P. K. Esselle, "Electromagnetic-wave beamscanning antenna using near-field rotatable graded-dielectric plates," *J. Appl. Phys.*, vol. 124, no. 23, pp. 912–915, 2018.
[16] M. U. Afzal, K. P. Esselle, and A. Lalbakhsh, "A metasurface to focus antenna beam at offset angle," in *Proc. 2nd URSI Atlantic Radio Sci. Meeting (AT-RASC)*, May 2018, pp. 1–4.
[17] P. Das, K. Mandal, and A. Lalbakhsh, "Single-layer polarization-insensitive frequency selective surface for beam reconfigurability of monopole antennas," *J. Electromagn. Waves Appl.*, vol. 34, no. 1, pp. 86–102, Jan. 2020.
[18] L. Song, W. Gao, C. O. Chui, and Y. Rahmat-Samii, "Wideband frequency reconfigurable patch antenna with switchable slots based on liquid metal and 3-D printed microfluidics," *IEEE Trans. Antennas Propag.*, vol. 67, no. 5, pp. 2886–2895, May 2019.
[19] S. Ahmed, F. A. Tahir, A. Shamim, and H. M. Cheema, "A compact kapton-based inkjet-printed multiband antenna for flexible wireless devices," *IEEE Antennas Wireless Propag. Lett.*, vol. 14, pp. 1802–1805, 2015.
[20] M. E. de Cos and F. Las-Heras, "Polypropylene-based dual-band CPW-fed monopole antenna," *IEEE Antennas Propag. Mag.*, vol. 55, no. 3, pp. 264–273, Jun. 2013.
[21] F. Faisal, Y. Amin, Y. Cho, and H. Yoo, "Compact and flexible novel wideband flower-shaped CPW-fed antennas for high data wireless applications," *IEEE Trans. Antennas Propag.*, vol. 67, no. 6, pp. 4184–4188, Jun. 2019.
[22] H. R. Raad, A. I. Abbosh, H. M. Al-Rizzo, and D. G. Rucker, "Flexible and compact AMC based antenna for telemedicine applications," *IEEE Trans. Antennas Propag.*, vol. 61, no. 2, pp. 524–531, Feb. 2013.

[23] H. R. Khaleel, H. M. Al-Rizzo, and D. G. Rucker, "Compact polyimide-based antennas for flexible displays," *J. Display Technol.*, vol. 8, no. 2, pp. 91–97, Feb. 2012.
[24] H. Liu, S. Zhu, P. Wen, X. Xiao, W. Che, and X. Guan, "Flexible CPW-fed fishtail-shaped antenna for dual-band applications," *IEEE Antennas Wireless Propag. Lett.*, vol. 13, pp. 770–773, 2014.
[25] G. Dattatreya and K. K. Naik, "A low volume flexible CPW-fed elliptical-ring with split-triangular patch dual-band antenna," *Int. J. RF Microw. Comput.-Aided Eng.*, vol. 29, no. 8, Aug. 2019.
[26] J. Jung, H. Lee, and Y. Lim, "Broadband flexible comb-shaped monopole antenna," *IET Microw., Antennas Propag.*, vol. 3, no. 2, pp. 325–332, Mar. 2009.
[27] H. R. Khaleel, H. M. Al-Rizzo, D. G. Rucker, and S. Mohan, "A compact polyimide-based UWB antenna for flexible electronics," *IEEE Antennas Wireless Propag. Lett.*, vol. 11, pp. 564–567, 2012.
[28] M. M. Bait-Suwailam and A. Alomainy, "Flexible analytical curve-based dual-band antenna for wireless body area networks," *Prog. Electromagn. Res. M*, vol. 84, pp. 73–84, Aug. 2019.
[29] S. M. Saeed, C. A. Balanis, and C. R. Birtcher, "Inkjet-printed flexible reconfigurable antenna for conformal WLAN/WiMAX wireless devices," *IEEE Antennas Wireless Propag. Lett.*, vol. 15, pp. 1979–1982, 2016.
[30] S. M. Saeed, C. A. Balanis, C. R. Birtcher, A. C. Durgun, and H. N. Shaman, "Wearable flexible reconfigurable antenna integrated with artificial magnetic conductor," *IEEE Antennas Wireless Propag. Lett.*, vol. 16, pp. 2396–2399, 2017.
[31] K. Saraswat and A. R. Harish, "Flexible dual-band dual-polarised CPW-fed monopole antenna with discrete-frequency reconfigurability," *IET Microw., Antennas Propag.*, vol. 13, no. 12, pp. 2053–2060, Oct. 2019.
[32] F. A. Tahir and A. Javed, "A compact dual-band frequency reconfigurable textile antenna for wearable applications," *Microw. Opt. Technol. Lett.*, vol. 57, no. 10, pp. 2251–2257, 2015.
[33] Z. Zhu, P. Wang, S. You, and P. Gao, "A flexible frequency and pattern reconfigurable antenna for wireless systems," *Prog. Electromagn. Res. Lett.*, vol. 76, pp. 63–70, 2018.
[34] A. Ahmad, F. Arshad, S. I. Naqvi, Y. Amin, H. Tenhunen, and J. Loo, "Flexible and compact spiral-shaped frequency reconfigurable antenna for wireless applications," *IETE J. Res.*, vol. 66, no. 1, pp. 22–29, Jan. 2020.
[35] H. F. Abutarboush and A. Shamim, "A reconfigurable inkjet-printed antenna on paper substrate for wireless applications," *IEEE Antennas Wireless Propag. Lett.*, vol. 17, no. 9, pp. 1648–1651, Sep. 2018.
[36] *IEEE Recommended Practice for Determining the Peak Spatial-Average Specific Absorption Rate(SAR) in the Human Head From Wireless Communication Devices: Measurement Techniques—Redline*, IEEE Standard 1528-2013 (Revision of IEEE Standard 1528-2003), 2013, pp. 1–500.

KODURI SREELAKSHMI received the B.Tech. degree in electronics and communication engineering (ECE) from JNTU Hyderabad, Telangana, India, and the M.Tech. degree in very large scale integration (VLSI) from JNTU Kakinada, Vishakapatnam, India. She is currently pursuing the Ph.D. degree (ECE) with Andhra University, Vishakapatnam. She has published six research articles in reputed international journals, such as springer, and so on. Her research interests include reconfigurable antennas, ultra-wideband antennas, and conformal antennas.

GOTTAPU SASIBHUSHANA RAO (Senior Member, IEEE) received the B.E. degree in electronics and communication engineering from Andhra University, Visakhapatnam, the M.Tech. degree (ECE) from JNTU, Hyderabad, the Ph.D. degree (ECE) from Osmania University, Hyderabad, and the M.B.A. degree (HRD & Marketing). He is currently working as a Professor with the Department of ECE, Andhra University College of Engineering, Visakhapatnam. He has 527 research publications and technical reports which include International/National Journals/ Conferences, such as the IEEE and Springer Journals and 18 technical reports submitted to DRDO, NSTL, UGC, CSIR, AICTE, and so on. He has 32 years of experience overall in teaching, research and development, and industry. He wrote textbooks on global navigation and satellite system (GNSS), mobile cellular communication, electromagnetic field theory and transmission lines, microwave and radar engineering. He is a Fellow of IETE.

M. N. V. S. S. KUMAR (Member, IEEE) received the B.Tech., M.Tech., and Ph.D. degrees from Andhra University. He is currently working as an Associate Professor with the Department of Electronics and Communication Engineering, Aditya Institute of Technology and Management, Tekkali. He completed two research projects funded by UGC and DLRL. He filed and published one patent. He published 110 research papers in various journals and conferences.